Sensitivity of Typhoon Track Predictions in a Regional Prediction System to Initial and Lateral Boundary Conditions

LING-FENG HSIAO

Central Weather Bureau, Taipei, Taiwan

MELINDA S. PENG

Marine Meteorology Division, Naval Research Laboratory, Monterey, California

DER-SONG CHEN, KANG-NING HUANG, AND TIEN-CHIANG YEH

Central Weather Bureau, Taipei, Taiwan

(Manuscript received 13 May 2008, in final form 25 December 2008)

ABSTRACT

Tropical cyclone (TC) track predictions from the operational regional nonhydrostatic TC forecast system of the Taiwanese Central Weather Bureau (CWB) are examined for their sensitivities to initial and lateral boundary conditions. Five experiments are designed and discussed, each using a combination of different initial and lateral boundary conditions coming either from the CWB or the National Centers for Environmental Prediction (NCEP) global forecast system. Eight typhoons in the western Pacific Ocean with 51 cases in 2004 and 2005 are tested with the five designed experiments for the 3-day forecast. The average track forecasts are the best when both the initial and lateral boundary conditions are from the NCEP global forecast system. This reflects the generally superior performance of the NCEP global forecast system relative to that of the CWB. Using different lateral boundary conditions has a greater impact on the track than using different initial conditions. Diagnostics using piecewise inversion of potential vorticity perturbations are carried out to identify synoptic features surrounding the featured typhoon that impact the track the most in each experiment. For the two cases demonstrated with the largest track improvement using NCEP global fields, the diagnostics indicate that the prediction of the strength and extent of the subtropical high in the western Pacific plays the major role in affecting these storm tracks. Using the analysis and predictions of the CWB global forecast system as the initial and lateral boundary conditions produces an overintensified subtropical ridge in the regional TC forecast model. Because most of the typhoons studied are located in the southwestern peripheral of the western Pacific subtropical high, the stronger steering from the more intense and extended high system is the main cause of the poleward bias in the predicted typhoon tracks in the operational run, which uses the CWB global forecast fields. The study suggests that, when efforts are made to improve a regional TC forecast model, it is also critically important to improve the global forecast system that provides the lateral boundary and initial conditions to the regional system.

1. Introduction

Taiwan, an island roughly 200 km wide and 400 km long centered at 23.5°N, 121°E, is frequently located along the routes of tropical cyclones (TCs, identified as typhoons in the region) in the western North Pacific Ocean. Typically, there are three to four typhoons making landfall in Taiwan each year, as published officially by the Central Weather Bureau (CWB) in Taiwan (information online at http://www.cwb.gov.tw.V5/information/knowledge/DATA/typhoon/ch2/040.html), posing significant threats to human lives and resulting in economic losses each year. Improving the prediction of typhoon tracks, intensity changes, as well as their accompanying wind and rainfall has the highest priority among tasks of the weather services in CWB and are also the main focus of atmospheric science research locally.

A high-resolution, nonhydrostatic regional forecast system (NFS) was developed and started as the operational forecast system at CWB in 2002 (Liou 2000).

Corresponding author address: Ling-Feng Hsiao, Central Weather Bureau, No. 64, Gongyuan Road, Taipei 10048, Taiwan.
E-mail: lfhsiao@rdc.cwb.gov.tw

DOI: 10.1175/2009JAMC2038.1

Report Documentation Page

Form Approved
OMB No. 0704-0188

1. REPORT DATE	2. REPORT TYPE	3. DATES COVERED
DEC 2008		**00-00-2008 to 00-00-2008**

4. TITLE AND SUBTITLE	5a. CONTRACT NUMBER
Sensitivity of Typhoon Track Predictions in a Regional Prediction System to Initial and Lateral Boundary Conditions	5b. GRANT NUMBER
	5c. PROGRAM ELEMENT NUMBER
6. AUTHOR(S)	5d. PROJECT NUMBER
	5e. TASK NUMBER
	5f. WORK UNIT NUMBER
7. PERFORMING ORGANIZATION NAME(S) AND ADDRESS(ES) **Naval Research Laboratory,Marine Meteorology Division,Monterey,CA,93943**	8. PERFORMING ORGANIZATION REPORT NUMBER
9. SPONSORING/MONITORING AGENCY NAME(S) AND ADDRESS(ES)	10. SPONSOR/MONITOR'S ACRONYM(S)
	11. SPONSOR/MONITOR'S REPORT NUMBER(S)

12. DISTRIBUTION/AVAILABILITY STATEMENT
Approved for public release; distribution unlimited

13. SUPPLEMENTARY NOTES

14. ABSTRACT
see report

15. SUBJECT TERMS

16. SECURITY CLASSIFICATION OF:			17. LIMITATION OF ABSTRACT	18. NUMBER OF PAGES	19a. NAME OF RESPONSIBLE PERSON
a. REPORT **unclassified**	b. ABSTRACT **unclassified**	c. THIS PAGE **unclassified**	**Same as Report (SAR)**	**17**	

When compared with the previous limited area model at CWB (Jeng et al. 1991), the NFS has better forecast scores and a reduced bias of excess precipitation existed in the previous model (Liou 2000). These are attributed in part to the improved parameterization of the subgrid-scale physical processes and better representation of the complex terrain in Taiwan. The NFS runs twice daily to provide routine forecasts for synoptic- and mesoscale weather systems. A CWB global forecast model (Liou et al. 1997) provides the initial and lateral boundary conditions (more discussion later) for the NFS. A version of NFS was also developed for the prediction of typhoons with a different domain and the inclusion of synthetic data to better represent the initial structure of a typhoon. This special-purpose forecast system runs only when a typhoon is in the vicinity of Taiwan. The TC forecast system using the NFS framework also improves the forecast track skill relative to the CWB typhoon forecast system based on the older limited-area forecast system (Peng et al. 1993; Chen et al. 2004, 2006). Efforts continue at CWB to improve the NFS in order to provide accurate subjective guidance for the forecast team. In this study, we investigate the sensitivity of typhoon track forecasts to the initial and lateral boundary conditions. From this point, the typhoon forecast system at CWB is referred as the NFS instead of introducing a new acronym.

Many factors contribute to forecast errors in numerical weather prediction systems. The growth of numerical forecast errors in some atmospheric weather regimes, or the transitions between two regimes, is inherently large, so that accurate and timely forecasts are often limited. Predictions of tropical cyclones suffer from lacking conventional data over open oceans where cyclones reside most of the time and lacking good estimation of the tropical cyclone structure at the initial stage. Krishnamurti et al. (1988) and Tiedtke et al. (1988) indicate that poor simulations of the timing, location, and intensity of precipitation in numerical prediction systems during the early spinup period of tropical cyclones come in part from inaccurate specification of the initial state of the atmosphere. Meanwhile, operational numerical prediction models have limitations on their grid resolutions and depend critically on the parameterization of subgrid-scale processes. Among the subgrid-scale processes, parameterizations for the planetary boundary layer and convection are most important to the simulation and prediction of tropical cyclones.

In general, a regional model uses either the analysis of a global model (cold start) or its own forecast fields from a previous data assimilation cycle as the first guess (update cycle) during data assimilation. Meanwhile, the lateral boundary conditions come from the forecast fields of a global model running ahead of the regional model in its operational phase. Through the initial and lateral boundary conditions, the forecast skill of a regional model depends on the accuracy of the global model, which may have less forecast skill due to a coarser resolution. Miguez-Macho and Paegle (2000) suggest that accurate initial and lateral boundary conditions for a regional model are the key elements for its success.

Studies have suggested that improving the initial states could improve the forecast skill of a numerical model. Langland et al. (2002) investigates the error growth and initial condition sensitivity for forecasts of January 2000 U.S. east coast snowstorms using singular vectors, adjoint sensitivity, and other techniques. It was demonstrated that the loss of forecast skills after 2 days stemmed mainly from the rapid growth of initial errors (identified by large growth of singular vectors) in the highly unstable regime. Several studies (Lorenz and Emanuel 1998; Palmer et al. 1998; Peng and Reynolds 2006) further identified areas where forecasts are most sensitive to initial perturbations by measuring the forecast sensitivity in terms of the total disturbance energy. Wu et al. (2005), using the framework of the fifth-generation Pennsylvania State University–National Center for Atmospheric Research Mesoscale Model (MM5), investigated the uncertainty of initial and lateral boundary conditions in a regional climate model and found that the lateral boundary forcing plays a critical role in the long-term regional climate modeling. The objective of this study is to study and evaluate the impacts of different initial conditions (the first-guess field in data assimilation) and lateral boundary conditions on the prediction of typhoon tracks in NFS. Experiments are designed to use a combination of different initial and lateral boundary conditions coming from either the CWB global forecast system (CWBGFS) that is used in operational runs, or the National Centers for Environmental Prediction (NCEP) global forecast system (NCEPGFS).

Initiated over warm oceans at low latitudes under favorable environmental conditions (Gray 1975; McBride and Zehr 1981), tropical cyclones generally move west and slightly northward in the early stages within the easterly trade winds and under the influence of the beta drift (Chan and Williams 1987; Fiorino and Elsberry 1989; Wang et al. 1997). Many environmental features, such as an approaching midlatitude trough, expansion or contraction of subtropical ridges, or the existence of another TC, may affect storm movements, resulting in a poleward recurving, quasi-stagnation, or even rotation about another storm (Elsberry 1987). In the final stages, they may transition into a midlatitude cyclone or make landfall and dissipate.

Many efforts have been devoted to understanding how environmental features affect TC motions. In most of these studies, the primary quantities used to examine TC motion are vorticity in a barotropic environment (Chan et al. 2002) or potential vorticity (PV) in a baroclinic environment (Shapiro 1996; Wu and Emanuel 1993). PV diagnostics have been proven useful in understanding synoptic- and large-scale dynamics due to their conservation following adiabatic and frictionless motion. For example, Molinari (1993) showed that the intensity changes of Hurricane Allen (1980) can be related to the evolution of an upper-tropospheric PV anomaly.

An innovative piecewise PV inversion scheme is developed by Davis and Emanuel (1991) using the nonlinear balance equation. The important feature of the piecewise inversion scheme is that the geopotential perturbations (and their derived wind fields) associated with individual PV anomalies are linearly superposable. Wu and Emanuel (1995a,b) use the piecewise PV inversion to study hurricane movement. Balanced flows associated with individual PV fields are found to be useful in explaining their contributions to the motions of tropical cyclones. Wu et al. (2003) use the PV-weighted distance between two coexisting TCs to illustrate the relative motion between them. To understand how different initial and lateral boundary conditions impact the storm track in the forecast model (NFS) from the dynamic perspective, piecewise inversion of the potential vorticity (Davis and Emanuel 1991) will be applied in this study.

The model description, the dataset used, and the design of our experiments are given in section 2. General experimental results are presented in section 3. Sections 4 and 5 contain the synoptic discussion and diagnostics using piecewise PV inversion for Typhoons Talim and Khanun, respectively. The summary is given in section 6.

TABLE 1. The vertical levels with sigma values in the terrain-following coordinates.

Level	σ
1	0.1
2	0.3
3	0.504
4	0.736
5	0.1004
6	0.1299
7	0.1621
8	0.1969
9	0.2343
10	0.2743
11	0.3170
12	0.3624
13	0.4103
14	0.4610
15	0.5143
16	0.5689
17	0.6232
18	0.6763
19	0.7273
20	0.7752
21	0.8193
22	0.8586
23	0.8922
24	0.9194
25	0.9392
26	0.9542
27	0.9674
28	0.9789
29	0.9886
30	0.9965

2. Experiments

a. Model description

The NFS is a nonhydrostatic primitive equation model with a fourth-order finite-difference scheme and positive-definite advection scheme for the moisture field (Hsu and Arakawa 1990). A split-explicit scheme is used for the time integration and a fourth-order diffusion is included to control grid-scale noises. Model physics used for this study include the Kuo scheme for cumulus parameterization (Kuo 1974), a simple cloud–ice explicit scheme for microphysics parameterization (Zhao et al. 1997) on the high-resolution grid, and a TKE–ε closure scheme for the planetary boundary layer processes. There are 30 vertical levels in the terrain-following vertical coordinate, with higher resolution assigned in the planetary boundary layer (Table 1). The optimal interpolation scheme is used for data assimilation.

While the NFS has the multiple-nesting capability, the forecast tracks from the three one-way nested domains with 45-, 15-, and 5-km horizontal grid spacings used operationally (Fig. 1) are very similar in general. However, predictions from the inner-most grid (5-km resolution) can provide better prediction of precipitation and wind fields over Taiwan with its more detailed terrain profile and microphysics. As we are focusing on the track forecast in this study, we will discuss and analyze results from the outer-most domain (45-km resolution) only. In addition, the design of the domain coverage is important for a regional model. Liang et al. (2001) demonstrates that the performance of a low-level jet event is significantly reduced when the southern boundary extends to the tropics, where large forcing errors exist. While it is desirable to have the regional forecast system covering as large an area as possible, significant tests have been carried out to finalize the

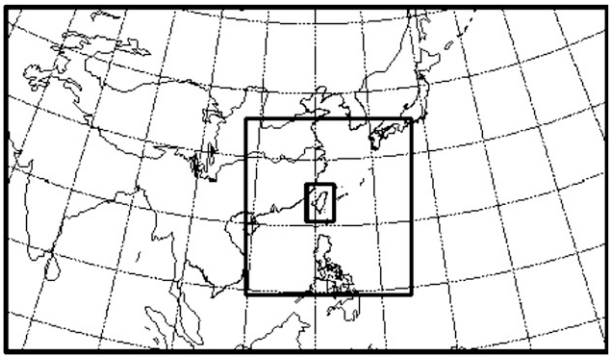

FIG. 1. Domain of the triple-nested NFS dedicated for operational tropical cyclone forecasts. Only the results from the outermost domain are discussed and analyzed.

optimal domain for operational runs of NFS as shown in Fig. 1.

CWBGFS is a spectral model with T179 resolution (approximately 1° resolution) and 30 vertical levels in the σ coordinate. For model physics, similarity theory is used to estimate the surface fluxes. A 1.5-order TKE–ε closure K theory is used to simulate the vertical turbulence mixing. The radiation scheme developed by Harshvardhan et al. (1987) is used in the model with the effects of H_2O, CO_2, and O_3. The cumulus parameterization uses the relaxed Arakawa–Schubert scheme formulated by Moothi and Suarez (1992). The model also includes large-scale precipitation and shallow convection.

The GFS [formerly the Aviation Model (AVN); Kanamitsu (1989)] is a global spectral data assimilation and forecast model system with production every 6 h at 0000, 0600, 1200, and 1800 UTC. Outputs from a horizontal grid spacing of approximately 1° × 1° and 42 vertical layers with a model top at 2 hPa are used in this study. In addition, the NCEP GFS does not use any synthetic bogus data for TC initialization except when the vortex is too weak in the first-guess field. More detailed documentations of the model can be found online (http://www.emc.ncep.noaa.gov/modelinfo).

The lateral boundary condition of the NFS is specified using the tendency of all variables from the global forecast fields with a blending zone covering seven grid points near the boundary of the NFS model domain. The representation of typhoons in the initial state is enhanced by first relocating the circulation associated with the storm to the observed position and then by including synthetic observations in the data assimilation (Liou 2004).

b. Datasets

In the operational run, the initial and lateral boundary conditions of the NFS are provided by the CWBGFS. Note that the amount of daily nontraditional observation data received from the Global Telecommunication System (GTS) at CWB is less than other major meteorology centers (including NCEP), due to the fact that Taiwan is not a member of the World Meteorology Organization, so that the observation data received at CWB are obtained from a private organization. On average, the surface synoptic observation (SYNOP) data are 15% less than those received at NCEP, the number of radiosonde observations (RAOBs) is about the same, and most of the satellite wind and vertical profiles are missing. While many factors contribute to the performance of a numerical model, such as the resolution and model physics, a shortage of data (particularly the satellite radiance) may be a significant one. Figure 2 is the comparison of the 500-hPa anomaly correlation coefficients between NCEPGFS and CWBGFS for the 1-, 2-, and 3-day forecasts in the Northern Hemisphere from May to September 2005. The NCEPGFS clearly shows more forecast skill (higher correlation) than the CWBGFS during the typhoon season, as well as in other seasons, and the difference is more pronounced for 72-h forecasts. In this study, we will examine how the performance of the global model impacts the forecasts of typhoon tracks in the NFS, with experiments using initial fields and lateral boundary conditions from CWBGFS and NCEPGFS, respectively, or a combination of both.

c. Experiment design

Five experiments were designed as listed in Table 2. The notation used in the experiments is specified in the following. The first letter denotes where the initial condition (the first guess in the data assimilation) comes from. A letter U indicates an update cycle, a C indicates a cold start with the first guess coming from CWBGFS, and an N indicates a cold start with the first guess coming from NCEPGFS. The second letter is expressed as a subscript as not all experiments need this notation. It represents an additional treatment in the initial first-guess field in certain areas. In the update cycle of the NFS, there are sometimes spurious small-scale low pressure systems over open oceans and over the Tibetan Plateau. These spurious lows cannot be removed by data assimilation because of the lack of observations. To remedy this, the data from CWBGFS are also used as bogus data over the ocean and over the Tibetan Plateau with 5° resolution in the data assimilation of the update cycle. This feature is denoted as the ''5° bogus'' in Table 2. This approach is adopted for the NFS as the general purpose regional forecast system and is also used in the operational TC forecast. In this study, this approach is evaluated further for the performance of TC predictions. Therefore, only experiments with an update cycle have a subscripted letter. The last letter indicates the source of the lateral

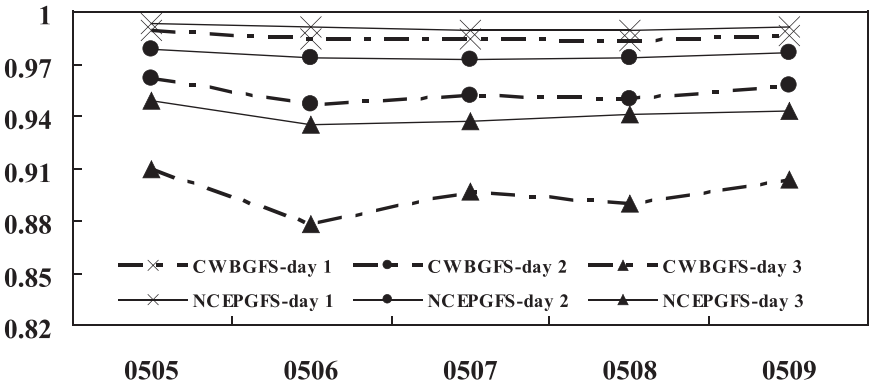

FIG. 2. Comparison of the anomaly correlation coefficient between the CWBGFS and NCEPGFS for the monthly averaged 1-, 2-, and 3-day forecasts from May to September 2005 in the Northern Hemisphere.

boundary condition, with C and N indicating the forecast fields from CWBGFS and NCEPGFS, respectively.

Following this notation, the control experiment is labeled as $U_C C$ with an update cycle for the first guess and lateral boundary conditions from CWBGFS. The forecasts from the $U_C C$ experiment are slightly different from those in the real-time operational runs due to the different observation dataset used in the latter that has an earlier data cutoff time. In experiment CC, both the initial fields and the lateral boundary conditions are from CWBGFS. In experiment NN, both the initial and lateral boundary data are from NCEPGFS. Experiment $U_N C$ is the same as $U_C C$ (operational run) except that the 5° bogus data over the ocean and the Tibetan Plateau area are from the NCEPGFS. Experiment $U_N N$ has the same initial conditions as in $U_N C$ while its lateral boundary conditions are from NCEPGFS.

All the integrations are carried out to 72 h.

3. Experiment results

Analysis of track errors

The NFS (the version dedicated for typhoon predictions) runs only when a typhoon is in the vicinity of Taiwan. There were 21 typhoons in 2004 and 2005 for which NFS has provided real-time forecasts. The average track errors of the real-time operational NFS for 24, 48, and 72 h are 112, 208, and 304 km, respectively, for all of the 191 cases of the 21 typhoons. Out of these storms, 51 cases for eight typhoons are chosen for our study (Table 3). These cases are the ones with poor performance from NFS during operational runs.

The 72-h-averaged track forecast distance errors from all five experiments are shown in Fig. 3. Note that the $U_C C$ (the control) results are very similar to the real-time operational runs. Among all the experiments, $U_N N$ has the best performance, followed closely by experiment NN. These experimental results indicate that using either initial field or lateral boundary conditions, or both, from NCEPGFS results in a better track prediction than using the CWBGFS fields. The comparison between $U_C C$ (operational run) and CC, where both use CWBGFS forecast fields as the lateral boundary conditions, indicates that a cold start is better than carrying the update cycle in NFS with the 5° bogus data from CWBGFS. This may, in part, provide the reason for the poorer forecasts in the 51 cases during operational runs. Meanwhile, keeping the update cycle and using the 5° bogus from CWBGFS does result in better performance than employing the cold start from CWBGFS completely. When the update cycle is kept while the data in the 5° bogus region are replaced by NCEPGFS analysis ($U_N C$), the forecast is slightly better than the control ($U_C C$). However, $U_N C$ is still inferior to CC without the update cycle of NFS. We are currently expanding our experiment sample size to determine whether a cold-start approach should be adopted in NFS for future operational runs.

Using forecast fields of NCEPGFS as the lateral boundary conditions (NN and $U_N N$) provides the best-track forecasts for our selected cases. Whether the NFS uses a

TABLE 2. Experimental designs using different initial and lateral boundary conditions.

	Initial conditions			
Expt	6-h update cycle	Cold start	5° bogus	Lateral boundary conditions
$U_C C$	Yes		CWBGFS	CWBGFS
CC		CWBGFS		CWBGFS
NN		NCEPGFS		NCEPGFS
$U_N C$	Yes		NCEPGFS	CWBGFS
$U_N N$	Yes		NCEPGFS	NCEPGFS

TABLE 3. The forecast dates and case numbers of eight typhoons of NFS with five experiments.

Typhoon	Forecast period	Case no.
Tokage	1200 UTC 14 Oct–0000 UTC 16 Oct 2004	4
Nesat	0000 UTC 3 Jun–0000 UTC 5 Jun 2005	5
Haitang	0000 UTC 12 Jul–1200 UTC 17 Jul 2005	12
Matsa	1200 UTC 31 Jul–1200 UTC 4 Aug 2005	8
Sanvu	1200 UTC 11 Aug–0000 UTC 13 Aug 2005	4
Talim	0000 UTC 28 Aug–1200 UTC 31 Aug 2005	8
Nabi	1200 UTC 29 Aug–1200 UTC 31 Aug 2005	5
Khanun	1200 UTC 7 Sep–1200 UTC 9 Sep 2005	5
Total no. of cases		51

cold start from NCEPGFS as its initial conditions or keeps its own update cycle with 5° bogus from NCEPGFS has little impact on the track forecasts.

In addition, Fig. 3 also contains the track errors from NCEPGFS and CWBGFS themselves. The track forecasts from NCEPGFS are clearly better than those from CWBGFS, fairly consistent with the comparison of their anomaly correlation coefficients in Fig. 2. The track errors from CWBGFS are the worst among all seven categories shown in Fig. 3. In the early stage of the forecast, the performance of the operational NFS is better than that of CWBGFS but is about the same in the later stage. On the other hand, the track simulation exhibited that NCEPGFS and U_NN are comparable. These comparisons further suggest the importance of the lateral boundary influence. Even though the high-resolution regional model has similar forecast skill in track prediction beyond 2 days, it does provide forecast skill in terms of typhoon-associated precipitation and winds. Many studies on numerical experiments demonstrate that a high-resolution mesoscale model can be a useful tool for typhoon prediction (Peng and Chang 2002; Wu et al. 2002; Wang 2007), mainly through a better, more detailed representation of the terrain profile and land–sea contours. For example, the maximum terrain heights on Taiwan are 2215, 2807.6, and 3271.6 m, in the 45-, 15-, and 5-km grid domains, respectively. In addition, a more sophisticated subgrid parameterization is used for fine grids that can better simulate the thermodynamics of typhoons.

For more detailed comparisons, Table 4 lists the percentage differences between two forecasts at different forecast times. As expected, different initial conditions generate large forecast differences in the early stages and the differences decrease with the forecast time. On the other hand, the differences increase with time with different lateral boundary conditions. A cold start from CWBGFS diminishes the 12-h forecast but improves the subsequent forecasts compared with the operational run (U_CC), where the update cycle is retained except in the 5° bogus region. Experiments U_CC and U_NC differ only in their initial data in the 5° bogus region, and their performance differences are small. Experiment U_NC shows significant improvement over CC for a 12-h

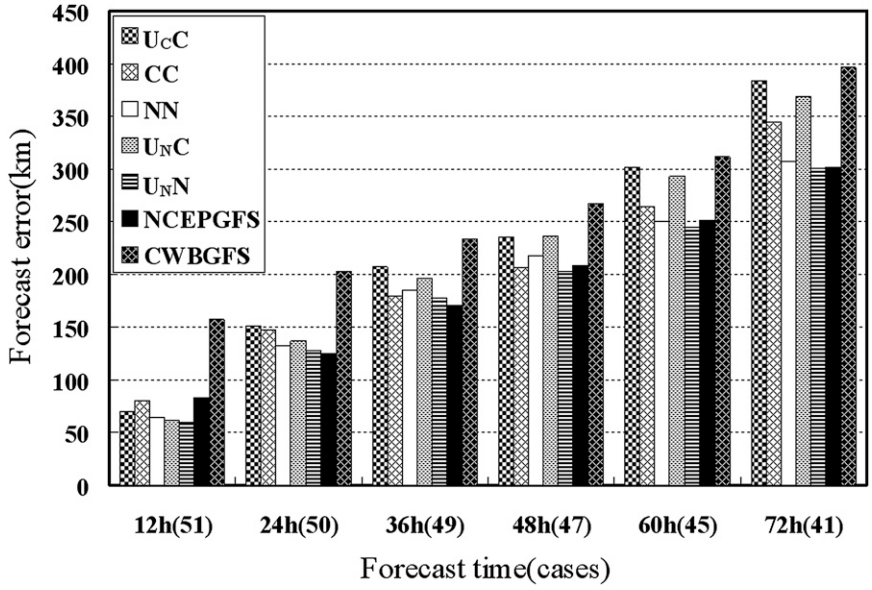

FIG. 3. The 72-h-averaged track errors of eight typhoons for 51 cases in 2004 and 2005.

TABLE 4. The differences (%) of the typhoon track errors among the different experiments.

Forecast time (h)	12	24	36	48	60	72
Different initial conditions						
$\frac{U_C C - CC}{U_C C}$	−16.4	2.7	13.4	12.5	12.5	10.4
$\frac{U_N C - CC}{U_N C}$	−31.1	−8.1	8.7	12.7	9.9	6.8
$\frac{U_N N - NN}{U_N N}$	−7.6	−3.9	−4.5	−7.4	−2.5	−2
$\frac{U_C C - U_N C}{U_C C}$	11.2	10	5.1	−0.3	2.9	3.9
Different lateral boundary conditions						
$\frac{U_N C - U_N N}{U_N C}$	3.3	5.9	9.7	14	16.7	18.4
Different initial and lateral boundary conditions						
$\frac{U_C C - U_N N}{U_C C}$	14.1	15.3	14.3	13.8	19.1	21.6

forecast (31.1%) but it forecasts trails CC at the later stage. As both experiments use the same lateral boundary conditions from the CWBGFS, it is not clear what causes the increase in the track errors beyond 12 h in U_NC. A more clean comparison for the effects of the initial conditions would be between U_CC and U_NC, where the only difference is the replacement of the data in the 5° bogus regions either by the CWBGFS analysis (U_CC) or by the NCEPGFS (U_NC). The U_NC is slightly better than the U_CC. Experiment U_NN performs better than NN for all forecasts, although the differences are very small.

Comparison between the experiment U_NC and U_NN highlights the clear effects of different lateral boundary conditions on the track forecasts. The improvement of the track using the NCEPGFS forecast fields as the lateral boundary conditions increases steadily with time. When the NCEPGFS analysis is used as the initial conditions (in the 5° bogus region) and forecast as the lateral boundary conditions, the largest improvement is obtained (U_CC versus U_NN). The differences in using different fields as the initial conditions are, in general, very small. One result that stands out with different initial conditions is that using the cold start from the CWBGFS is better than keeping the update cycle with blending of the initial field, except at 12 h, as discussed previously.

Based on the superior performance of the NCEPGFS over CWBGFS, using the NCEPGFS analysis as the initial conditions and its forecasts as the lateral boundary conditions (instead of CWBGFS) improves the typhoon track forecast in NFS. In the following section, we diagnose the synoptic fields of the forecasts and the steering flow associated with individual components of the atmospheric circulation to identify features leading to the improvement of the track forecast in different experiments.

Among the eight storms studied, the forecast of Typhoon Talim has the largest average track error, 484 km at 72 h, in the operational run. This large forecast error for Talim contributes significantly to the total track error for NFS for the season. Because of its poor performance, one case starting on 29 August 2005 was chosen as a case study for the PV diagnostics. Another case chosen for individual study is Typhoon Khanun, with the forecast starting at 1200 UTC 17 September 2005. These two cases are discussed in the following sections.

4. Analysis for Typhoon Talim

a. Synoptic fields

Talim first formed northwest of Guam on 27 August. As it moved west-by-northwest in the early stage, its intensity increased. Subsequently, Talim moved to the northwest and then passed through the center part of Taiwan to the Fujian Provence of mainland China. The best track and model forecasts of Talim starting at 0000 UTC 29 August are shown in Fig. 4. All of the forecasts for the track have a northwestward bias. In particular, the U_CC (operational) run has the largest track error. Experiment U_NC has the least improvement over U_CC, where the only difference from U_CC is in the use of the NCEPGFS analysis data in the 5° bogus region. When the first guess uses a cold start from the CWBGFS and the lateral boundary conditions from the CWBGFS (CC), a slight improvement in the track forecast is obtained. Experiments NN and U_NN improve the track forecasts more significantly with the lateral boundary conditions coming from NCEPGFS and the initial conditions coming either totally from the NCEPGFS (NN) or partially from NCEPGFS within the 5° bogus region only (U_NN). The track distance errors are 91, 214, and 305 km and 92, 202, and 303 km, respectively, from NN and U_NN experiments for the 24-, 48-, and 72-h forecasts, as compared with 48, 208, and 549 km in U_CC.

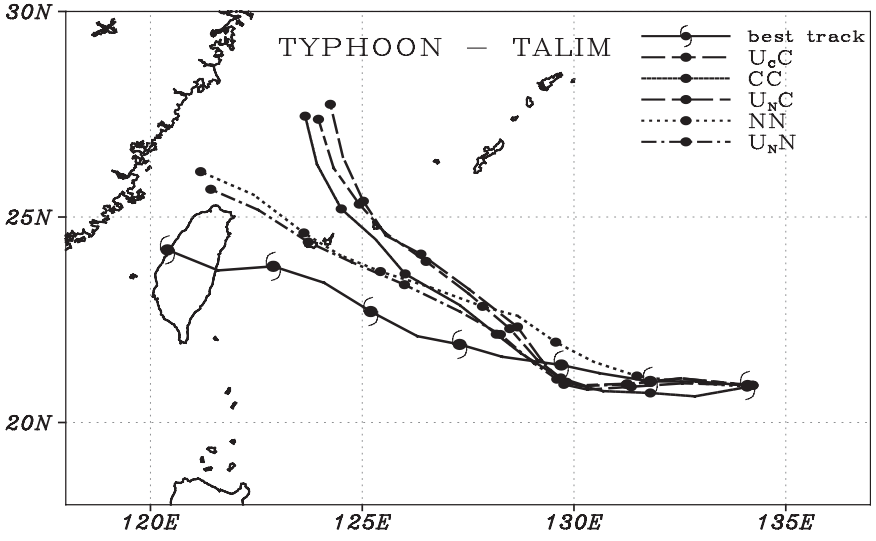

FIG. 4. The track forecast of Talim 0000 UTC 29 Aug–1 Sep from the five experiments. The heavy solid line with typhoon symbols is the CWB best track. Each symbol represents the typhoon center every 12 h.

Note that while the forecast track distance errors for U_NN and NN are very close at 24 h, the directions are different with the U_NN forecast track to the right of the best track and the NN forecast to the left.

The results of our experiments indicate that using both the initial and the lateral boundary conditions from NCEPGFS improves most of the forecast tracks of Talim, with different lateral boundary conditions having the largest impact in the extended forecast. This is consistent with the average of the all cases discussed in section 3. Figure 5 shows the 500-hPa geopotential height from the NCEP analysis during the simulated period from 0000 UTC 29 August to 0000 UTC 1 September. Talim was located to the southwest of the subtropical high between 0000 UTC 29 August and 0000 UTC 30 August. The western flank of the high weakens slightly while its intensity increases after 1200 UTC 30 August. The weakening of the subtropical high may be a result of the intrusion of Talim. During the same period, the trough to the north (between 30° and 40°N) intensified between 29 and 30 August, and a cutoff low formed at 1200 UTC 30 August (shown on 31 August). Meanwhile, another typhoon (Nabi) appeared to have formed in the wake of Talim (Fu et al. 2007) and moved along with Talim. For comparison, Fig. 6 contains the 500-hPa geopotential height of the forecast fields at the 48- and 72-h forecasts (valid on 31 August and 1 September) from the two global models, CWBGFS and NCEPGFS, respectively. The analysis fields from both systems have small differences, with the subtropical ridge stronger in the CWBGFS while Talim was more intense in the NCEPGFS analysis (figure not shown). For the 48-h forecast, the subtropical ridge intensified further in the CWBGFS forecast (Fig. 6a) than in the NCEPGFS forecast (Fig. 6b). The trough to the northwest became a cutoff low in both systems with the one in the NCEPGFS slightly more intense. At the 72-h forecast, the CWBGFS that provides the lateral boundary conditions to the U_CC has a more intense trough, relative to the forecast in NCEPGFS. The 48- and 72-h forecasts of the 500-hPa geopotential height fields from U_CC and U_NN are given in Fig. 7. With the influence from the lateral boundary, the characteristics of the forecasts of the overall synoptic systems are very similar between U_CC and CWBGFS and between U_NN and NCEPGFS, respectively. The trough to the northwest of Talim is more intense in and CWBGFS than in U_NN and NCEPGFS. Meanwhile, the forecasts of the subtropical ridge are also more intense in U_CC and CWBGFS than in U_NN and NCEPGFS. In the next section, we use piecewise PV inversion to identify the major steering responsible for the movement of Talim in different experiments.

b. Piecewise PV diagnosis

The piecewise PV inversion technique was developed by Davis (1992). Conceptually, this technique separates the potential vorticity field into individual pieces bearing different synoptic patterns in different regions. The nonlinear balance equation is then solved for each individual PV field to retrieve the wind field associated with each PV field. The purpose of applying this approach in our study is to identify which and how each individual PV anomaly contributes to the typhoon motion in different experiments. The symmetric average

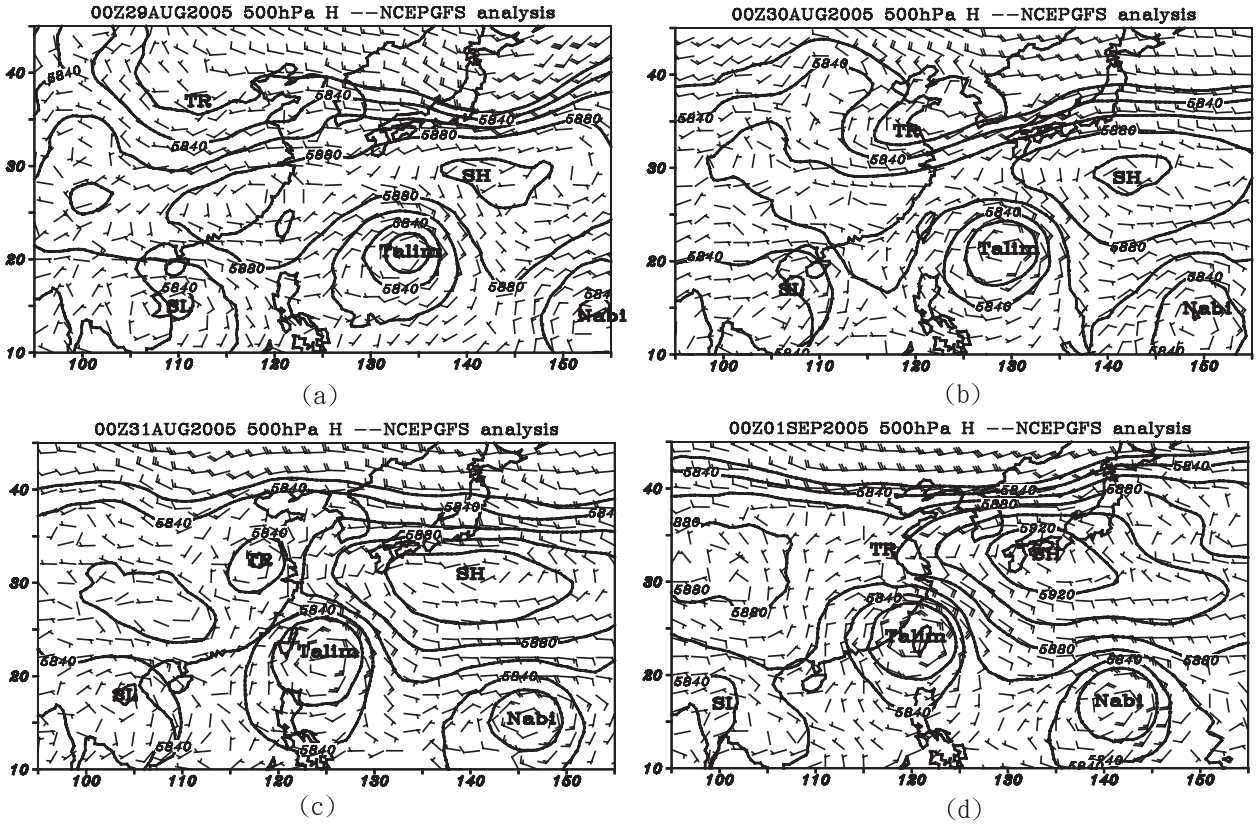

FIG. 5. Geopotential height and wind fields of the NCEPGFS analysis at 500 hPa 0000 UTC 29 Aug–0000 UTC 1 Sep.

with respect to the typhoon center is treated as the mean field and the piecewise PV inversion is carried out for different parts of the disturbance, as in Wu and Emanuel (1995a,b) and Shapiro (1996). The balance equation is, in spherical coordinates,

$$\nabla^2\Phi = \nabla\cdot(f\nabla\Psi) + \frac{2}{a^4\cos^2\phi}\frac{\partial(\Psi_\lambda,\Psi_\varphi)}{\partial(\lambda,\phi)},$$

where Φ is the geopotential height, Ψ is the streamfunction of the nondivergent flow, a is the earth's radius, f is the Coriolis parameter, λ is the latitude, and ϕ is the longitude. The PV field is calculated by the following formula:

$$q = -\frac{gk\pi}{p}\left(\eta\frac{\partial\theta}{\partial\pi} - \frac{1}{a\cos\phi}\frac{\partial v}{\partial\pi}\frac{\partial\theta}{\partial\lambda} + \frac{1}{a}\frac{\partial u}{\partial\pi}\frac{\partial\theta}{\partial\phi}\right),$$

where $\kappa = R_d/C_p$ and $\pi = C_p(p/p_0)^\kappa$ is the vertical coordinate, η is the vertical component of the absolute vorticity, and the hydrostatic approximation is with $\theta = -\partial\Phi/\partial\pi$. The total field is separated into the mean and perturbation parts, where the mean is the axisymmetric average centered at the storm and the perturbation is the deviation from the mean. The perturbation PV is then separated into different components associated with different synoptic features in different regions (see the example below). The piecewise PV inversion retrieves the nonlinear balanced mass field associated with individual PV perturbations. The steering flows associated with individual PV disturbances for the cyclone are then computed from the retrieved wind fields. The typhoon advection flow is defined as the balanced flow at the storm center associated with the total PV distribution, excluding the positive PV anomaly of the storm itself. The steering flow ($\mathbf{V}$) is computed as the deep-layer-mean wind vector between 925 and 300 hPa averaged within a 3° latitude circle around each typhoon center (note that we have used 5° latitude as the range and the results are similar); that is,

$$\mathbf{V} = \frac{\int_{925\text{hPa}}^{300\text{hPa}}\mathbf{V}_S(p)\,dp}{\int_{925\text{hPa}}^{300\text{hPa}}dp} \quad \text{and}$$

$$\mathbf{V}_S(p) = \frac{\int_0^{3^\circ}\int_0^{2\pi}\mathbf{V}r\,dr\,d\theta}{\int_0^{3^\circ}\int_0^{2\pi}r\,dr\,d\theta}.$$

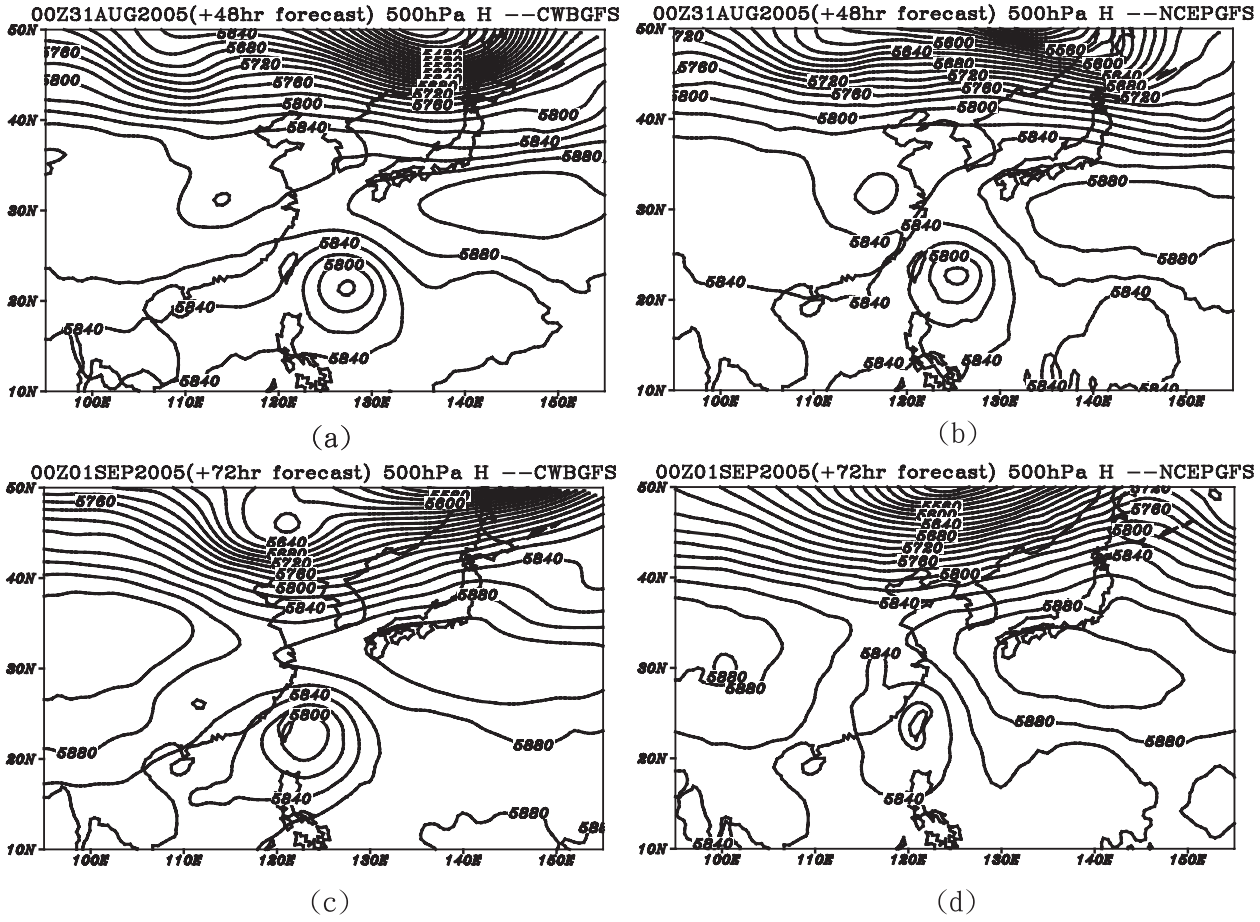

FIG. 6. Geopotential height at 500 hPa at (a) 0000 UTC 31 Aug (48-h forecast) from CWBGFS, (b) 0000 UTC 31 Aug (48-h forecast) from NCEPGFS, (c) 0000 UTC 1 Sep (72-h forecast) from CWBGFS, and (d) 0000 UTC 1 Sep (72-h forecast) from NCEPGFS.

Our experimental results discussed previously show that different initial fields and lateral boundary conditions can affect the prediction of typhoon tracks in the NFS model. In this section, we apply the piecewise PV inversion to diagnose the impact of different synoptic systems on the prediction of Typhoon Talim (Fig. 4), of which the operational NFS shows the worse typhoon track forecast in 2005. Our diagnostics are intended to find out what impacts the track forecasts most, using the piecewise PV inversion technique.

For the piecewise PV inversion diagnostics of Talim, the total perturbation PV field is divided into four separate regions associated with the subtropical high (SH) in the western Pacific, the midlatitude trough (TR) to the northwest, Typhoon Nabi to the southeast, and the low over the South China Sea (SL) (Fig. 8). These are the major features near Typhoon Talim that may impacts its movement. The five experiments listed in Table 3 for Typhoon Talim at 0000 UTC 29 August are analyzed by the piecewise PV inversion diagnosis.

The time series of the best track [$\mathbf{V}_{BT}$, $\mathbf{V}_{BT} = (\mathbf{X}_{t+6} - \mathbf{X}_{t-6})/12$ h, where $\mathbf{X}_{t-6}$ ($\mathbf{X}_{t+6}$) is the storm center 6 h earlier (6 h later)], and the steering flow computed from four individual PV perturbations and the total perturbation for experiments $U_C C$ and $U_N N$, are shown in Fig. 8, as $U_N N$ provides the greatest improvement on the track forecast, and we use its forecasts and those from the $U_C C$ for our diagnostics only. The PV perturbations includes the SH, the TR, the SC, Tropical Cyclone Nabi, and the total PV perturbation. First, we compare the steering vector from the total PV perturbation field (q') with the best track ($\mathbf{V}_{BT}$). While there are angle differences between the steering and the best track, mainly due to the beta effect (Holland 1983), the steering vectors are, in general, in good agreement with the tracks. There are substantial differences between the best-track movement vectors and the steering vectors from the forecasts of $U_C C$ from 0000 UTC 30 August to 1 September, with the best-track wind vector mostly westward while the steering from the $U_C C$

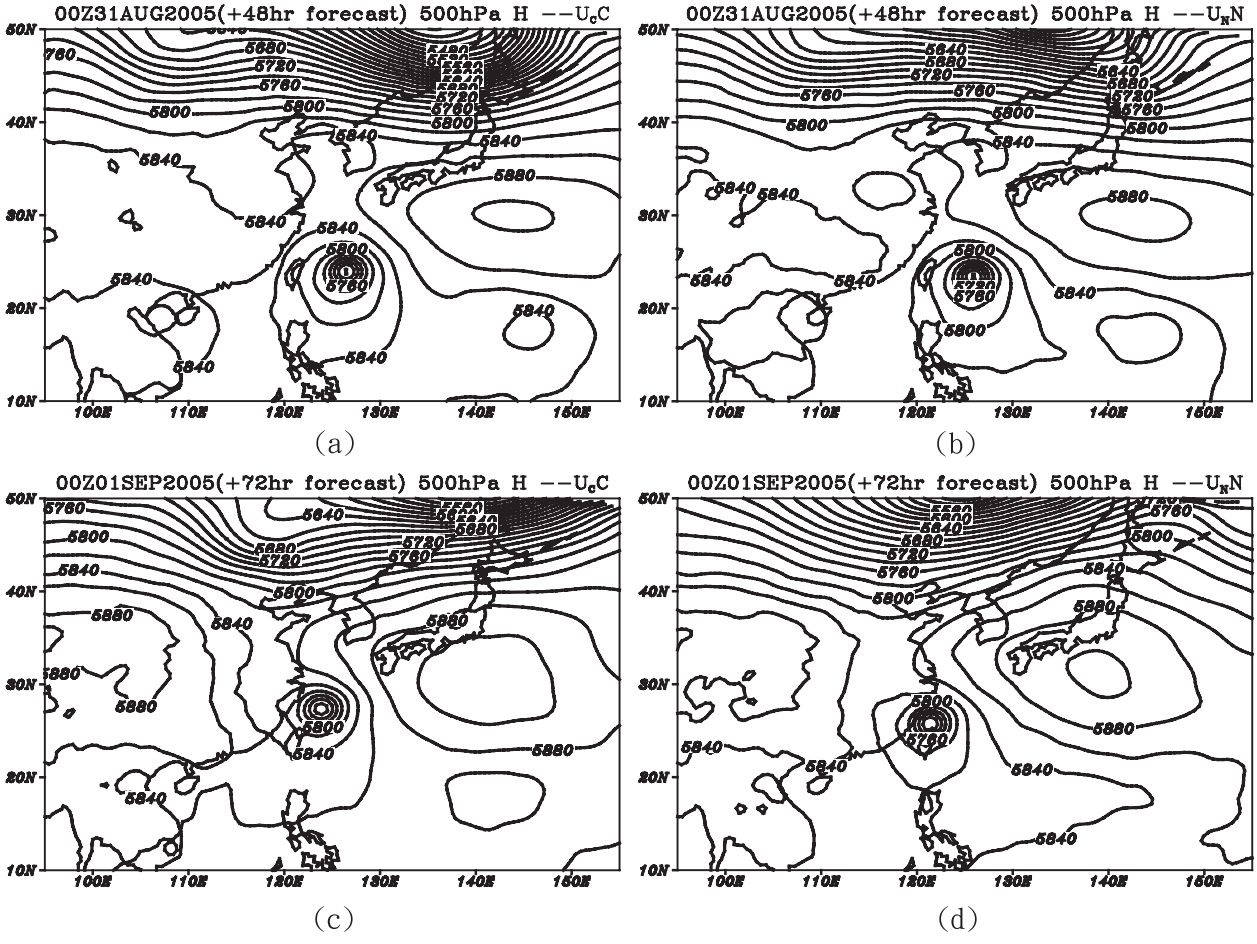

FIG. 7. The (top) 48- and (bottom) 72-h forecast from the (left) $U_C C$ and (right) $U_N N$ for the 500-hPa geopotential height starting at 0000 UTC 29 Aug.

has a large northward component. The northward steering in $U_C C$ causes large northward bias in its forecast track (Fig. 4). Meanwhile, the total perturbation in experiment $U_N N$ has a steering flow that is in better agreement with the best-track movement vector and it is reflected by its superior forecast of the track (Fig. 4).

Next, we examine the steering vector from individual PV perturbations associated with the SH, TR, SL, and Nabi. The steering vectors from the PV perturbation associated with Nabi and SL are very similar in $U_C C$ and $U_N N$. They both are small and apparently make little contribution to the total steering of Talim. The steering vectors associated with the midlatitude trough (TR) from $U_C C$ and $U_N N$ are different, especially at 1200 UTC 30 August and 0000 UTC 31 August when the deviation between the $U_C C$ and the $U_N N$ is distinct. Comparing the steering vectors associated with the four individual perturbations with the steering of the total disturbance indicates that the major component of the total steering comes from the one associated with the SH. The two steering vectors from the total disturbance of $U_C C$ and $U_N N$ have large angle differences between them, mainly coming from the steering associated with the SH with some contribution from the steering associated with the TR. On average, the magnitude of the steering vector $\mathbf{V}_{SH}$ is about twice that of the $\mathbf{V}_{TR}$. Overall, the similarity between the $\mathbf{V}_{SH}$ and $\mathbf{V}_{q'}$ indicates that the total steering is dominated by the SH and both the SH and TR contribute to the steering of the total disturbance at 1200 UTC 31 August and 1 September. Note that the total steering vector is much weaker than the best-track steering from both $U_C C$ and $U_N N$ on 30 August. This is the time when Talim made the curvature.

In summary, using different initial and lateral boundary conditions in NFS has a large impact on the forecast of the subtropical high that steered Talim. During the period where the track from the $U_C C$ has a large northward bias, both the steering vectors associated with the midlatitude trough (TR) and the subtropical high (SH) from the $U_C C$ have larger southerly components,

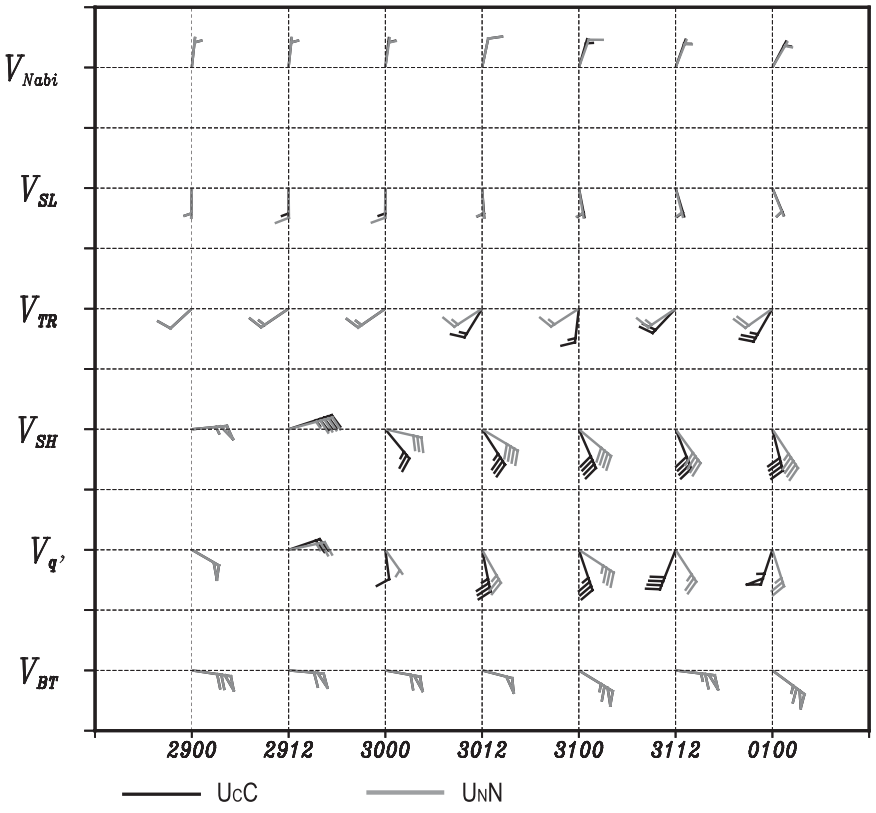

FIG. 8. Time series (0000 UTC 29 Aug–1 Sep) of the movement of Talim (2005) and the steering flow associated with the PV perturbation of the total ($\mathbf{V}_{q'}$), SH, TR, SL, and Nabi components for experiments U_CC (black) and U_NN (gray). One full barb represents 1 m s^{-1} and one flag is 5 m s^{-1}.

contributing to the southerly component of the total steering in the U_CC. Meanwhile, the steering vectors in U_NN have smaller southerly components and are mostly from the east. The different steerings from both the subtropical high and the midlatitude trough in U_CC and U_NN contributes to the difference in the total steering that leads to the superior forecast track for Talim in U_NN over the U_CC.

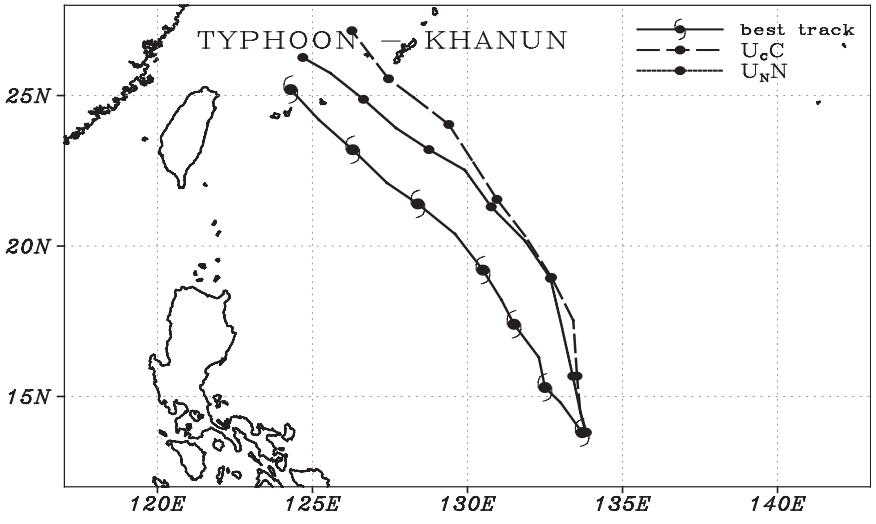

FIG. 9. The track forecast of Khanun at 1200 UTC 7–10 Sep from U_CC and U_NN. The heavy solid line is the CWB best track. Each symbol represents the typhoon center every 12 h.

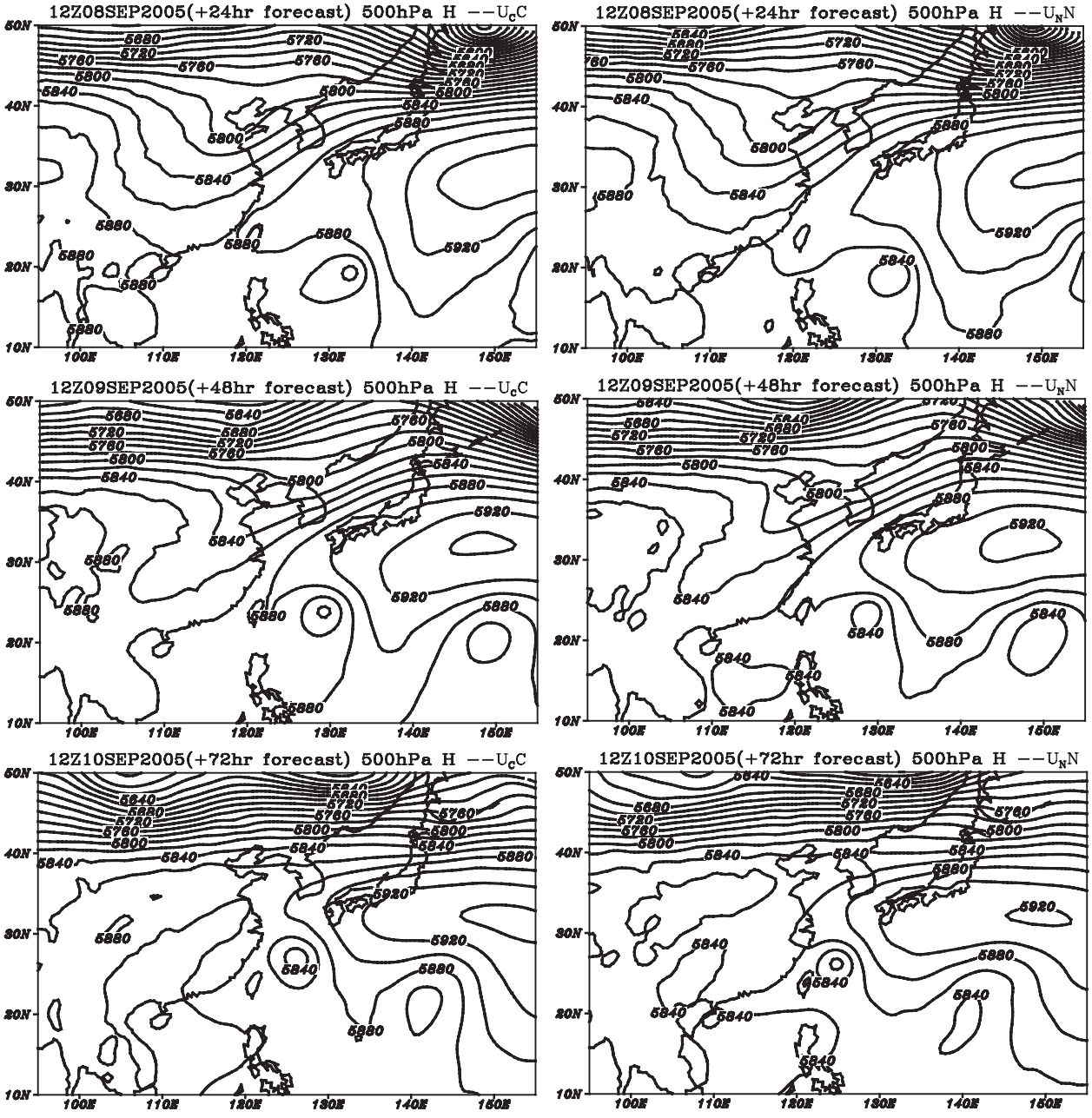

FIG. 10. (top to bottom) The 1–3-day forecast of the 500-hPa geopotential height starting at 1200 UTC 7 Sep from (left) U_CC and (right) U_NN.

5. Diagnostics for Typhoon Khanun

To further illustrate the impacts of the initial and lateral boundary conditions on the track forecast, the PV diagnostics are carried out for the prediction of Khanun at 1200 UTC 7 September 2005. The best track and the forecast track from U_CC and U_NN are given in Fig. 9. There is little different between the tracks from U_CC and U_NN before 36 h (0000 UTC 9 September). The U_CC track continues its poleward-biased movement while the track from U_NN deviates from the U_CC and its distance error is improved from 303 km in U_CC to 118 km at 72 h. We will see if the PV diagnostics reflect the similarities of the two experiments before 36 h and the deviation afterward.

The forecast 1–3-day synoptic 500-hPa geopotential heights from U_CC and U_NN are presented in Fig. 10. The major differences between these two forecasts are the

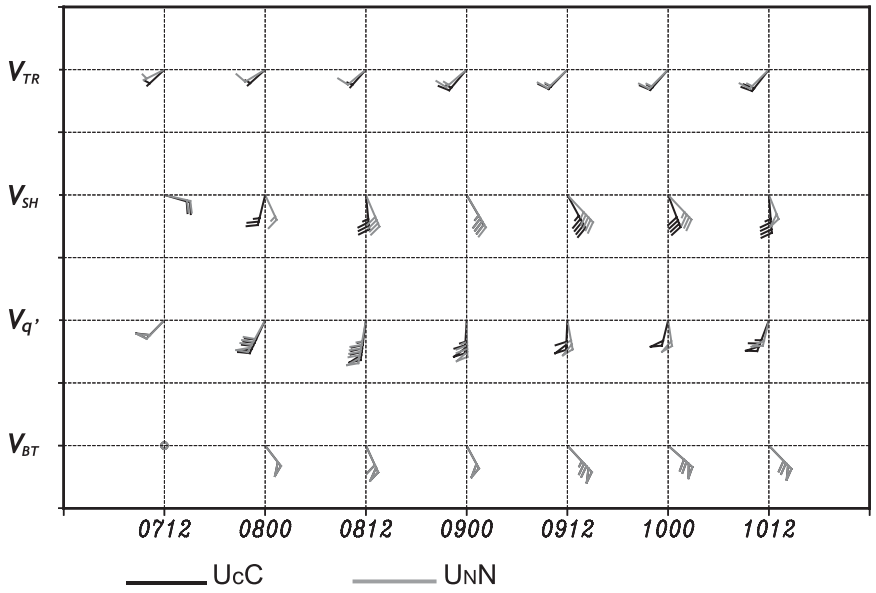

FIG. 11. As in Fig. 8, but for Typhoon Khanun (2005) at 1200 UTC 7–9 Sep with two PV disturbances associated with the trough and the subtropical high.

stronger subtropical high in U_CC, especially on days 2 and 3, and a slightly stronger trough in U_NN on days 1 and 2. In this case, we only separate the total disturbance into the subtropical high and the midlatitude trough, as there is no other appreciable system nearby. The piecewise PV diagnostics is given in Fig. 11. The steering vectors of the total disturbance ($\mathbf{V}_{q'}$) from U_CC and U_NN have almost the same direction up to the 36-h forecast (valid at 0000 UTC 9 September). This corresponds well with the similar forecast tracks between U_CC and U_NN during the same period (Fig. 9). The two total-steering vectors separate after 36 h with the one from U_NN having more of a westward component. The major differences in the steering components come from the one associated with the subtropical high ($\mathbf{V}_{SH}$). The steering vectors associated with the trough ($\mathbf{V}_{TR}$) from the two experiments are very similar, especially in the later stage. Their contributions to the total disturbance are also small.

This case and the case presented for Talim demonstrate that the environmental synoptic-scale features play important roles in affecting the movement of tropical cyclones. In general, the strength of the subtropical high system has a large impact on the storm tracks in the western Pacific. This may change for different cases and in different seasons.

6. Summary

Accurate predictions of tropical cyclones are critical for countries annually affected by tropical cyclones. In this study, we demonstrate that the performance of the regional prediction system for tropical cyclone tracks (the NFS) at the Central Weather Bureau in Taiwan depends critically on the initial conditions (used as the first guess in the data assimilation) and the lateral boundary conditions. Operational NFS uses the initial and lateral boundary conditions from the CWB global forecast system (CWBGFS). In our experiments, a combination of different initial and lateral boundary conditions coming either from the CWBGFS or the NCEP global model (NCEPGFS) are used. Among all of the experiments, the one using both the initial and lateral boundary conditions from the NCEPGFS shows the largest improvement over the operational run. This is not surprising as the NCEPGFS has a better overall forecast score than the CWBGFS, while the latter suffers significantly from having less observational data received at the CWB. The different initial conditions only have a small impact in the early stage and different lateral boundary conditions have a large impact on forecasts beyond 36 h. This is true even though the regional model covers a fairly large domain.

In summary, using initial and lateral boundary conditions from a global model with better forecast skill can significantly improve the prediction of typhoon tracks in a regional model. The PV diagnostics for two cases, using the piecewise inversion technique, indicate that the lateral boundary conditions impact the prediction of the intensity and extent of the subtropical high in the western Pacific and steering from the subtropical high plays the major role in affecting the movement of the two typhoons

studies. This may change for different typhoon cases for storms with different sizes/intensities, and at different geographical locations.

Our study suggests that using the update cycle of the NFS to set the initial conditions does not perform better than using a cold start from CWBGFS and it will be recommended for operational consideration. This study indicates that, in order to improve the forecasts of tropical cyclones in a regional high-resolution model, efforts have to be taken to improve the global forecast system that provides the lateral boundary conditions (and initial conditions) as well.

Acknowledgments. This study was supported by the National Science Council of the Republic of China under Grants NSC94-2119-M-052-001-Ap1 and NSC95-2119-M-052-001-Ap1. The data and the computation resources were provided by the Central Weather Bureau. We are grateful to Prof Chun-Chieh Wu for helping with our piecewise potential vorticity inversion analysis. The authors also thank the two anonymous reviewers for their constructive comments and suggestions on the manuscript.

REFERENCES

Chan, J. C. L., and R. T. Williams, 1987: Analytical and numerical studies of the beta-effect in tropical cyclone motion. Part I: Zero mean flow. *J. Atmos. Sci.,* **44,** 1257–1265.

——, F. M. F. Ko, and Y. M. Lei, 2002: Relationship between potential vorticity tendency and tropical cyclone motion. *J. Atmos. Sci.,* **59,** 1317–1336.

Chen, D. S., L. F. Hsiao, K. N. Huang, and T. C. Yeh, 2004: A study on the impact of initial fields on the typhoon track and rainfall simulation in the vicinity of Taiwan. Preprints, *26th Conf. on Hurricanes and Tropical Meteorology,* Miami, FL, Amer. Meteor. Soc., 15C.5. [Available online at http://ams.confex.com/ams/pdfpapers/75851.pdf.]

——, ——, ——, and ——, 2006: An experiment on the impact of initial fields and boundary conditions on the typhoon track simulation in the northwest Pacific Ocean. Preprints, *27th Conf. on Hurricanes and Tropical Meteorology,* Monterey, CA, Amer. Meteor. Soc., 11A.7. [Available online at http://ams.confex.com/ams/pdfpapers/107421.pdf.]

Davis, C. A., 1992: Piecewise potential vorticity inversion. *J. Atmos. Sci.,* **49,** 1397–1411.

——, and K. A. Emanuel, 1991: Potential vorticity diagnostics of cyclogenesis. *Mon. Wea. Rev.,* **119,** 1929–1953.

Elsberry, R. L., Ed., 1987: *A Global View of Tropical Cyclones*. Office of Naval Research, 185 pp.

Fiorino, M., and R. L. Elsberry, 1989: Some aspects of vortex structure related to tropical cyclone motion. *J. Atmos. Sci.,* **46,** 975–990.

Fu, B., T. Li, M. S. Peng, and F. Weng, 2007: Analysis of tropical cyclogenesis in the western North Pacific for 2000 and 2001. *Wea. Forecasting,* **22,** 763–780.

Gray, W. M., 1975: Tropical cyclone genesis. Dept. of Atmospheric Science Paper 232, Colorado State University, Fort Collins, CO, 121 pp.

Harshvardhan, R. Davies, D. A. Randall, and T. G. Corsetti, 1987: A fast radiation parameterization for atmospheric circulation models. *J. Geophys. Res.,* **92,** 1009–1016.

Holland, J., 1983: Tropical cyclone motion: Environmental interaction plus a beta effect. *J. Atmos. Sci.,* **40,** 328–342.

Hsu, Y.-J. G., and A. Arakawa, 1990: Numerical modeling of the atmosphere with an isentropic vertical coordinate. *Mon. Wea. Rev.,* **118,** 1933–1959.

Jeng, B.-F., H.-J. Chen, S.-C. Lin, T.-M. Leou, M. S. Peng, S. W. Chang, W.-R. Hsu, and C.-P. Chang, 1991: The Limited-Area Forecast Systems at the Central Weather Bureau. *Wea. Forecasting,* **6,** 155–178.

Kanamitsu, M., 1989: Description of the NMC Global Data Assimilation and Forecasting System. *Wea. Forecasting,* **4,** 335–342.

Krishnamurti, T. N., H. S. Bedi, W. Heckley, and K. Ingles, 1988: Reduction of the spinup time for evaporation and precipitation in a spectral model. *Mon. Wea. Rev.,* **116,** 907–920.

Kuo, H. L., 1974: Further studies of the parameterization of the influence of cumulus convection on large-scale flow. *J. Atmos. Sci.,* **31,** 1232–1240.

Langland, R. H., M. A. Shapiro, and R. Gelaro, 2002: Initial condition sensitivity and error growth in forecasts of the 25 January 2000 East Coast Snowstorm. *Mon. Wea. Rev.,* **130,** 957–974.

Liang, X.-Z., K. E. Kunkel, and A. N. Samel, 2001: Development of a regional climate model for U.S. Midwest applications. Part I: Sensitivity to buffer zone treatment. *J. Climate,* **14,** 4363–4378.

Liou, C.-S., 2000: On the improvement of quantitative precipitation forecast by CWB numerical forecast systems around Taiwan. CWB Rep. CWB89-6M-02, 338 pp.

——, 2004: Improving forecast of rainfall and strong wind associated with typhoons approaching Taiwan. CWB Rep. CWB93-3M-01, 318 pp.

——, and Coauthors, 1997: The second-generation Global Forecast System at the Central Weather Bureau in Taiwan. *Wea. Forecasting,* **12,** 653–663.

Lorenz, E. N., and K. A. Emanuel, 1998: Optimal sites for supplementary weather observations: Simulation with a small model. *J. Atmos. Sci.,* **55,** 399–414.

McBride, J. L., and R. Zehr, 1981: Observational analysis of tropical cyclone formation. Part II: Comparison of nondeveloping versus developing systems. *J. Atmos. Sci.,* **38,** 1132–1151.

Miguez-Macho, G., and J. Paegle, 2000: Sensitivity of a global forecast model to initializations with reanalysis datasets. *Mon. Wea. Rev.,* **128,** 3879–3889.

Molinari, J., 1993: Environmental controls on eye wall cycles and intensity change in Hurricane Allen (1980). *Proc. ICSU/WMO Int. Symp. on Tropical Cyclone Disasters,* Beijing, China, World Meteorological Organization, 328–337.

Moothi, S., and M. J. Suarez, 1992: Relaxed Arakawa–Schubert: A parameterization of moist convection for general circulation models. *Mon. Wea. Rev.,* **120,** 978–1002.

Palmer, T. N., R. Gelaro, J. Barkmeijer, and R. Buizza, 1998: Singular vectors, metrics, and adaptive observations. *J. Atmos. Sci.,* **55,** 633–653.

Peng, M. S., and S. W. Chang, 2002: Numerical forecasting experiments on Typhoon Herb (1996). *J. Meteor. Soc. Japan,* **80,** 1325–1338.

——, and C. A. Reynolds, 2006: Sensitivity of tropical cyclones forecasts as revealed by singular vectors. *J. Atmos. Sci.,* **63,** 2508–2528.

——, B.-F. Jeng, and C.-P. Chang, 1993: Forecast of typhoon tracks in the vicinity of Taiwan during 1989–1990 using a dynamical model. *Wea. Forecasting,* **8,** 309–325.

Shapiro, L. J., 1996: The motion of Hurricane Gloria: A potential vorticity diagnosis. *Mon. Wea. Rev.,* **124,** 2497–2508.

Tiedtke, M., W. A. Heckley, and J. Slingo, 1988: Tropical forecasting at ECMWF: The influence of physical parameterization on the mean structure of forecasts and analyses. *Quart. J. Roy. Meteor. Soc.,* **114,** 639–664.

Wang, B., X. Li, and L. Wu, 1997: Direction of hurricane beta drift in horizontally sheared flows. *J. Atmos. Sci.,* **54,** 1462–1471.

Wang, Y., 2007: A multiply nested, movable mesh, fully compressible, nonhydrostatic tropical cyclone model—TCM4: Model description and development of asymmetries without explicit asymmetric forcing. *Meteor. Atmos. Phys.,* **97,** 93–116.

Wu, C.-C., and K. A. Emanuel, 1993: Interaction of a baroclinic vortex with background shear: Application to hurricane movement. *J. Atmos. Sci.,* **50,** 62–76.

——, and ——, 1995a: Potential vorticity diagnostics of hurricane movement. Part I: A case study of Hurricane Bob (1991). *Mon. Wea. Rev.,* **123,** 69–92.

——, and ——, 1995b: Potential vorticity diagnostics of hurricane movement. Part II: Tropical Storm Ana (1991) and Hurricane Andrew (1992). *Mon. Wea. Rev.,* **123,** 93–109.

——, T.-H. Yen, Y.-H. Kuo, and W. Wang, 2002: Rainfall simulation associated with Typhoon Herb (1996) near Taiwan. Part I: The topographic effect. *Wea. Forecasting,* **17,** 1001–1015.

——, T. S. Huang, W. P. Huang, and K. H. Chou, 2003: A new look at the binary interaction: Potential vorticity diagnosis of the unusual southward movement of Tropical Storm Bopha (2000) and its interaction with Supertyphoon Saomai (2000). *Mon. Wea. Rev.,* **131,** 1289–1300.

Wu, W., A. H. Lynch, and A. Rivers, 2005: Estimating the uncertainty in a regional climate model related to initial and lateral boundary conditions. *J. Climate,* **18,** 917–933.

Zhao, Q., T. L. Black, and M. E. Baldwin, 1997: Implementation of the cloud prediction scheme in the Eta Model at NCEP. *Wea. Forecasting,* **12,** 697–713.